Fluid-wall interactions in a deformable system

Sergueï KORNELIK[(1,2)], Salah NAILI[(1)],
Christian ODDOU[(1)], Alexï BOUBENTCHIKOV[(2)]

[(1)]Laboratoire de Mécanique Physique, B2OA UMR 7052 CNRS
Université Paris XII, Val-de-Marne,
Faculté des Sciences et Technologie,
61, Avenue du Général de Gaulle,
94010 Créteil cédex, France.

E-mail : naili@univ-paris12.fr, oddou@univ-paris12.fr

[(2)]Chair of the Mathematical Analysis,
Tomsk's State University,
Faculty of Applied Mechanics and Mathematics,
Russia, 634040, Tomsk, ul. Prospekt Lenina, 36.

E-mail : kornelik@tbs.ru

European Physics Journal – Applied Phycics
Editor: Professor C. Colliex
39 pages, 9 figures
3 copies submitted

September 9, 2002 at 08h28

Fluid-wall interactions in a deformable system

Corresponding author

Salah NAILI
Laboratoire de Mécanique Physique, CNRS UMR 7052 — B2OA
Université Paris XII, Val-de-Marne,
Faculté des Sciences et Technologie,
61, Avenue du Général de Gaulle,
94010 Créteil cédex, France.

Tel. : 33 1 45 17 14 45
Fax. : 33 1 45 17 14 33

E-mail : naili@univ-paris12.fr

Abstract — The purpose of this work is the modeling and the analysis of fluid-wall interactions in a deformable cylindrical cavity which has one single orifice for inflow and outflow. The model is used to study the dynamical behavior of a non linear oscillatory coupled system. Indeed, the deformation of the cavity can be large, therefore the fluid containt inside the cavaty changes greatly. Our analysis describes the behavior of the system according to its characteristic parameters. A dimensional analysis of the set of coupled equations describing the dynamical behavior of both the incompressible fluid and the cavity wall is performed. We show that such a behavior can be characterized by five dimensionless parameters. The equations are then solved by using the so-called *time-staggered* scheme which allows to integrate separately the equations describing the structure and the fluid dynamics during each time step. The fluid part is discretized by the finite difference method associated with an Arbitrary Lagrangian Eulerian formulation of the governing fluid dynamics equations and the structure part including the motion of the piston by a Runge-Kutta method. For an harmonic excitation, we show that after a transient phase, the response of the system is both anharmonic and periodic, with a fundamental period equal to that of the excitation. Moreover, we study the respective influence of the wall rigidity, the fluid viscosity and the inertia effects, for different magnitudes of the excitation. Using an approximation of the damping force associated with the viscous effects of the dynamical flow, we complete this study by showing how the system of equations can be decoupled.

NOMENCLATURE

Geometrical variables

$\mathbf{B}_T$	:	fixed frame supporting the envelope
$\mathcal{D} = \mathcal{D}_1 \cup \mathcal{D}_2$	:	domain containing the fluid
$\Gamma_2, \Gamma_3, \Gamma_4$	:	lateral fixed walls
Γ_5	:	surface of the rigid piston
Γ_6	:	axis of symmetry
R_1, R_2, L_1, L_2	:	radii and lengths of the cavity
S_1, S_2	:	cross-sectional area of the domains $\mathcal{D}_1$ and $\mathcal{D}_2$
x, r, θ	:	cylindrical coordinates
$\vec{e}_x$	:	unit vector of the cavity axis

Fluid-dependent variables

ρ	:	fluid density
μ	:	dynamic viscosity
$\overrightarrow{U}$	:	fluid velocity
U_x, U_r	:	axial and radial components of the fluid velocity
$\tilde{U}_1, \tilde{U}_2$	:	average speeds at the cross sections of the domains $\mathcal{D}_1$ and $\mathcal{D}_2$
Ω	:	azimuthal component of the vorticity
ψ	:	stream function

Wall-dependent variables

k : rigidity of the spring

ω : frequency of excitation

γ : elongation of the spring

U_p : velocity of the piston

Force variables

$\overrightarrow{T}$: sum of the stress vectors of external forces

$\overrightarrow{T_{\Gamma_i}}$: force exerted by the fluid on a fixed frame $\mathbf{B}_T$ supporting the envelope at its boundary Γ_i where $i = 2, 3$

$\overrightarrow{T_{\Gamma_5}}$: force exerted by the spring on the piston

$\overrightarrow{T^(1)_{\Gamma_4}}$: force exerted by the fluid on a fixed frame $\mathbf{B}_T$ supporting the envelope at its boundary Γ_4

$\overrightarrow{T^(2)_{\Gamma_4}}$: force exerted by the frame $\mathbf{B}_T$ on the piston defined by the boundary Γ_4

p_e : mean pressure imposed at the input-output of the cavity

$p_e(t), p_p(t)$: average pressures of the fluid on sections Γ_1 and Γ_3

p_m, p_a : constant pressures

f_f : axial component of damping force due to the action of the wall on the fluid

Scheme-dependent variables

W_x, W_r : axial and radial components of the mesh velocity

$h_1, h_2(t)$: step lengths of spatial discretization in the x directions

h_r : step length of spatial discretization in the r directions

Dimensionless characteristic parameters

α : Womersley's parameter or unsteady Reynolds number

K : normalized rigidity

P_a : normalized amplitude of the external unsteady pressure

D_r : average dilatation of $\mathcal{D}$

S : area ratio

Fluid-wall interactions in a deformable system

Sergueï KORNELIK, Salah NAILI,

Christian ODDOU & Alexï BOUBENTCHIKOV

September 9, 2002 at 08h28

I— Introduction

Research on coupled phenomena has recently known a rapid expansion and numerous applications in offshore engineering [see, *e.g.* Boderick & Leonard (1995)], aeroelasticity [see, *e.g.* Guruswamy (1988)] and biomechanics [see, *e.g.* Heil (1998)]. Fluid-wall interactions are one of these coupled phenomena that involve the circulation of a fluid in a deformable envelope. In this process the dynamics of the solid and fluid components are mutually dependent upon the conditions imposed on the common interface. Thus, in these systems the dynamics of the envelope depends on the fluid flow, and reciprocally, the fluid flow depends on the shape and the motion of this envelope. For instance, in cardio-vascular system the interest is focused on the motion of vortex in deformable cavity in which a fluid is injected because the detection of such an abnormal flow pattern may be of clinical interest. This pattern is generally associated with thrombus formation in the apical area. Delamarre *et al.* (1987) detected the motion of vortex in human dilated ventricles by using Doppler echocardiography. During the filling phase, this vortex starts at the mitral valve and progresses through the left ventricular cavity

towards the apex. In this context, to define a model in order not only to produce but also to convect by diffusion a vortex while that the global stiffness of the wall is a stake relevant. Therefore, the values of the parameters of this study have been selected so as to correspond to the physical situation involved in cardiovascular systems.

The present paper is focused on the delicate problem of the fluid-wall coupling when a single opening is used as inlet or outlet for the fluid. We propose a new Arbitrary Lagrangian Eulerian (ALE) description of the equations describing the dynamic behavior of the fluid in its vorticity-stream function version. This version is associated with a method of numerical resolution that is able to take into account the fluid-wall interactions for large displacements. In this case, the mass of fluid contained in the cavity changes by large amounts. Moreover, we will emphasise in this study a dimensional analysis showing that the dynamics of the system is governed by five dimensionless characteristic parameters. Furthermore, this work contributes to the study of strongly non linear and oscillating coupled systems. The analysis reports on the dynamic behavior of such systems in function of the most influential characteristic parameters.

We consider a deformable cylindrical cavity with a sudden expansion in which an unsteady flow of a viscous incompressible fluid is generated by pressurization through one of its ends. At the other extremity, the cavity is limited by a mobile rigid and massless piston connected to a spring. The system of coupled equations were solved by applying the so-called *time-staggered* scheme which

allows to integrate separately the equations describing the structure and the fluid during each time step [see, *e.g.* Piperno *et al.* (1996)]. The fluid part is discretized by the finite difference method associated with an Arbitrary Lagrangian Eulerian formulation [see, *e.g.* Hughes *et al.* (1981)] of the governing fluid dynamic equations. The structure part defining the motion of the piston is solved by a RUNGE-KUTTA method. In the range of values of the studied parameters and after a transient phase, we have shown that for an harmonic excitation, the response of the system — characterized by the movement of the piston — is periodic and anharmonic, at the frequency of the excitation. Moreover, with the numerical tests, we study the respective influence of the wall rigidity, modeled by a spring elasticity, the fluid viscosity and inertia effects according to the intensity of the excitation. Using an approximation of the damping force which is associated with the viscous effects of the dynamical flow, we have also shown how the set of equations can be decoupled.

II — Formulation of the problem

The system studied in this work, as shown Fig. 1, is a cylindrical cavity where an unsteady incompressible viscous flow is generated by pressurization at one of its extremities. At the other side there is a mobile piston connected to a spring, whose rigidity k is assumed constant. Since the fluid content in this cavity varies with time, one can consider this system as a deformable cavity. The cavity lateral wall is fixed to the frame and the mobile piston is considered to have a negligible mass.

Figure 1 gives the notations related to the geometry of the system. Its dynamics can be presented in the following way: (i) the difference in pressure between sections Γ_1 and Γ_5 puts the fluid under motion, (ii) the action of the fluid on section Γ_5 exerts a deformation on the spring, (iii) this deformation induces a new difference in pressure, (iv) so that the cycle restarts in (i).

II.1 — Motion of the piston

Neglecting the body forces per unit mass and summing the two equations derived from the fundamental principle of dynamics applied successively to the domain $\mathcal{D}$ containing the fluid and to the envelope defined by both the cavity and the piston, we get the relation:

$$\frac{d}{dt}\int_{\mathcal{D}} \rho \overrightarrow{U}\, dv = \int_S \overrightarrow{T}\, dS, \tag{1}$$

where ρ designates the fluid density, $\overrightarrow{U}$ its velocity, $\overrightarrow{T}$ is the sum of the stress vectors of external forces acting on the surface S limiting the domain $\mathcal{D}$, dv and dS are the differential elements of volume and surface respectively.

The sum of the exterior mechanical actions exerted on the domain $\mathcal{D}$ and the envelope is given by:

$$\int_S \overrightarrow{T}\, dS = p_e(t) S_1 \vec{e}_x - \overrightarrow{T_{\Gamma_2}} - \overrightarrow{T_{\Gamma_3}} - \overrightarrow{T^{(1)}_{\Gamma_4}} + \overrightarrow{T_{\Gamma_5}} + \overrightarrow{T^{(2)}_{\Gamma_4}}, \tag{2}$$

where $\vec{e}_x$ is the unit vector of the cavity axis, p_e stands for the mean pressure imposed at the input-output of the cavity, S_1 is the cross sectional area of the domain $\mathcal{D}_1$, $\overrightarrow{T_{\Gamma_i}}$ designates the force exerted by the fluid on a fixed frame $\mathbf{B}_T$

supporting the envelope at its boundary Γ_i with $i = 2, 3$, $\overrightarrow{T_{\Gamma_5}}$ the force exerted by the spring on the piston, $\overrightarrow{T^{(1)}_{\Gamma_4}}$ the force exerted by the fluid on a fixed frame $\mathbf{B}_T$ supporting the envelope at its boundary Γ_4 and $\overrightarrow{T^{(2)}_{\Gamma_4}}$ the force exerted by the frame $\mathbf{B}_T$ on the piston defined by the boundary Γ_4.

We suppose that the piston's movement along the wall Γ_4 is frictionless, *i.e.* $\overrightarrow{T^{(2)}_{\Gamma_4}} \cdot \vec{e}_x = 0$. A simple calculation enables us to determine each term of the right hand side of equation (2), by using the continuity of the stress vectors as well as the velocities of the fluid and the envelope on the interface, which is a simple consequence of the no-slip condition. The axial component of the expression (2) gives the following relation:

$$\int_S \overrightarrow{T} \cdot \vec{e}_x dS = p_e(t)S_1 + f_f(t) + p_p(t)(S_2 - S_1) - k\gamma, \tag{3}$$

where S_2 designates the cross sectional area of the domain $\mathcal{D}_2$, k the rigidity of the spring, f_f the damping force due to the action of the wall on the fluid in the axial direction, γ the elongation of the spring, and finally, $p_e(t)$ and $p_p(t)$ are the average pressures of the fluid on sections Γ_1 and Γ_3 respectively.

The damping force f_f, due to viscous effects, is determined by the stress vector, resulting from the action of the wall on the fluid. The axial component of this force is given by the following relation:

$$f_f(t) = 2\pi\mu \left\{ R_1 \int_0^{L_1} \frac{\partial}{\partial r} U_x(x, r, t) \mid_{r=R_1} dx + R_2 \int_{L_1}^{L(t)} \frac{\partial}{\partial r} U_x(x, r, t) \mid_{r=R_2} dx \right\}, \tag{4}$$

where U_x designates the axial component of the fluid velocity, μ the dynamic viscosity and $L(t) = L_1 + L_2 + \gamma(t)$.

We next introduce a weighted average of the pressures defined by:

$$p(t) = p_e(t) + (\frac{R_2^2}{R_1^2} - 1)p_p(t), \tag{5}$$

whose form is chosen in such a way that $p(t) = p_m + p_a \sin(\omega t - \pi/2)$, where p_m and p_a are given constants, and ω the excitation frequency. This choice means that the longitudinal force resulting from the pressure and normal stresses acting on $\mathcal{D}$ is imposed.

The left hand-side of equation (1) is given by:

$$\frac{d}{dt}\int_{\mathcal{D}} \rho \overrightarrow{U}\, dv = \frac{d}{dt}\int_{\mathcal{D}_1} \rho \overrightarrow{U}\, dv + \frac{d}{dt}\int_{\mathcal{D}_2} \rho \overrightarrow{U}\, dv. \tag{6}$$

Owing to the flow incompressibility hypothesis, the flow-rates are equal at each cross-section; then we have the following equations:

$$S_1\tilde{U}_1 = S_2\tilde{U}_2 = S_2\frac{d\gamma}{dt},$$

where $\tilde{U}_1$ and $\tilde{U}_2$ denote the average speeds at the cross sections of the domains $\mathcal{D}_1$ and $\mathcal{D}_2$ respectively.

Thus, the axial component of the relation (6) gives:

$$\frac{d}{dt}\int_{\mathcal{D}} \rho \overrightarrow{U} \cdot \vec{e}_x\, dv = \frac{d}{dt}\left\{\rho S_2 L_1 \frac{d\gamma}{dt}\right\} + \frac{d}{dt}\left\{\rho S_2 (L_2 + \gamma)\frac{d\gamma}{dt}\right\}. \tag{7}$$

To carry out an analysis using dimensionless variables, we introduce the following notations:

$$\bar{t} = \omega t,\ \bar{x} = \frac{x}{L_0},\ \bar{r} = \frac{r}{L_0},\ \bar{L}_1 = \frac{L_1}{L_0},\ \bar{L}_2 = \frac{L_2}{L_0},\ \bar{R}_1 = \frac{R_1}{L_0},\ \bar{R}_2 = \frac{R_2}{L_0}, \tag{8a}$$

$$\bar{p} = \frac{p}{\rho L_0^2 \omega^2},\ \bar{f}_f = \frac{f_f}{\mu L_0^2 \omega},\ \bar{\gamma} = \frac{\gamma}{L_0},\ \bar{\gamma}_0 = \frac{\gamma_0}{L_0},\ \bar{U}_x = \frac{U_x}{L_0 \omega},\ \bar{U}_r = \frac{U_r}{L_0 \omega}, \qquad (8b)$$

with $L_0 = L_1 + L_2 + \gamma_0$ and $\gamma_0 = \pi R_1^2 \frac{p_m}{k}$, where γ_0 is an average elongation of the spring which corresponds to the equilibrium state of the system.

In this case, the axial component of the relation (1) becomes :

$$\frac{d}{d\bar{t}} \left\{ (\bar{L}_1 + \bar{L}_2 + \bar{\gamma}(\bar{t})) \frac{d\bar{\gamma}}{d\bar{t}} \right\} - \frac{1}{\pi \bar{R}_2^2 \alpha^2} \bar{f}_f(\bar{t}) + K(\bar{\gamma} - \bar{\gamma}_0) = S P_a \sin(\bar{t} - \pi/2). \quad (9a)$$

This relation can be interpreted as describing the motion of the piston, where in our problem, the piston represents the massless mobile part of the cavity structure. It should be noted that this result can be obtained from the alternative form:

$$K(\bar{\gamma} - \bar{\gamma}_0) = \bar{P} \bar{S}_2, \qquad (9b)$$

where $\bar{P}$ is a dimensionless average pressure acting on the piston. Indeed, by applying the fundamental principle of dynamics to the domain $\mathcal{D}$, one can show that equation $(9b)$ is equivalent to equation $(9a)$.

The dimensional analysis of equation $(9a)$ allows to introduce dimensionless characteristic parameters:

$$\alpha = L_0 \sqrt{\frac{\rho \omega}{\mu}},\ K = \frac{k}{\rho \pi R_2^2 L_0 \omega^2},\ P_a = \frac{p_a}{\rho L_0^2 \omega^2}, \qquad (10a)$$

$$D_r = \frac{R_2^2 \gamma_0}{L_1 R_1^2 + (L_2 + \gamma_0) R_2^2},\ S = \frac{R_1^2}{R_2^2}. \qquad (10b)$$

The parameter α, called Womersley's parameter or the unsteady Reynolds number, represents the ratio between the unsteady effects of inertia and the viscosity effects. The normalized rigidity K represents the ratio between the

capacity of the deformation and the unsteady inertial effects of the fluid. To obtain the resonance frequency, it is sufficient to vary this parameter so as to describe the response spectrum. This spectrum goes from oscillations at low frequency — *i.e.* inertia negligible compared to the spring force — into those of high frequency — *i.e.* dominated by inertial effects. The parameter associated with the normalized amplitude of the external unsteady pressure P_a represents the ratio between the external forces and the unsteady inertial effects. Finally, the geometrical parameter D_r expresses an average dilatation of $\mathcal{D}$; while S is a parameter associated with the overall geometry of the system.

II.2 — Description of the fluid dynamics

II.2.a — ALE formulation of Navier-Stokes equation

The determination of $\bar{f}_f$ requires the knowledge of the velocity field of the fluid at each time. This field is obtained by solving the equations of the fluid dynamics in a vorticity-stream function formulation [see, *e.g.* Guyon *et al.* (1991)], noted $(\Omega - \psi)$, associated with an Arbitrary Lagrangian Eulerian description [see, *e.g.* Hughes *et al.* (1981)]. The system of equations describing the flow, in dimensionless variables $(\bar{\Omega} - \bar{\psi})$, owing to the axial symmetry, is given by:

$$\frac{\partial \bar{\Omega}}{\partial \bar{t}} + \frac{\partial \bar{\Omega}\bar{V}_x}{\partial \bar{x}} + \frac{\partial \bar{\Omega}\bar{V}_r}{\partial \bar{r}} - \frac{\partial \bar{W}_x}{\partial \bar{x}}\frac{\partial \bar{U}_x}{\partial \bar{r}} + \frac{\partial \bar{W}_r}{\partial \bar{r}}\frac{\partial \bar{U}_r}{\partial \bar{r}} - \frac{\partial \bar{W}_r}{\partial \bar{x}}\frac{\partial \bar{U}_r}{\partial \bar{r}} + \frac{\partial \bar{W}_x}{\partial \bar{x}}\frac{\partial \bar{U}_x}{\partial \bar{x}} = \frac{1}{\alpha^2}\left\{\frac{\partial^2 \bar{\Omega}}{\partial \bar{x}^2} + \frac{\partial}{\partial \bar{r}}\left(\frac{1}{\bar{r}}\frac{\partial \bar{r}\bar{\Omega}}{\partial \bar{r}}\right)\right\}, \tag{11a}$$

$$\frac{1}{\bar{r}}\frac{\partial^2 \bar{\psi}}{\partial \bar{x}^2} + \frac{\partial}{\partial \bar{r}}\left(\frac{1}{\bar{r}}\frac{\partial \bar{\psi}}{\partial \bar{r}}\right) = -\bar{\Omega}, \tag{11b}$$

$$\bar{U}_x = \frac{1}{\bar{r}}\frac{\partial \bar{\psi}}{\partial \bar{r}}, \quad \bar{U}_r = -\frac{1}{\bar{r}}\frac{\partial \bar{\psi}}{\partial \bar{x}}, \quad \bar{\Omega} = \frac{\partial \bar{U}_r}{\partial \bar{x}} - \frac{\partial \bar{U}_x}{\partial \bar{r}}, \tag{12a}$$

$$\bar{V}_x = \bar{U}_x - \bar{W}_x, \quad \bar{V}_r = \bar{U}_r - \bar{W}_r, \tag{12b}$$

$$\bar{W}_x = \bar{W}_r = 0, \quad \text{in } \mathcal{D}_1 \tag{13a}$$

$$\bar{W}_x = \frac{d\bar{\gamma}}{d\bar{t}} \frac{(\bar{x} - \bar{L}_1)}{(\bar{\gamma} + \bar{L}_2)}, \quad \forall \bar{x} \in [\bar{L}_1, \bar{L}(\bar{t})] \text{ and } \bar{W}_r = 0, \quad \text{in } \mathcal{D}_2 \tag{13b}$$

where $\bar{\Omega}$ designates the azimuthal component of the vorticity, $\bar{\psi}$ the stream function, $\bar{U}_x$ and $\bar{U}_r$ the longitudinal and radial components of the fluid velocity respectively, $\bar{W}_x$ and $\bar{W}_r$ the corresponding components of the mesh velocity.

II.2.b — Boundary conditions

For the sake of simplicity, we write the boundary conditions on the domain $\mathcal{D}$, omitting the bars on the dimensionless variables.

The following relations have to be satisfied on Γ_1:

$$\frac{\partial \psi}{\partial x} = 0, \quad \text{and} \quad \Omega = -\frac{\partial}{\partial r}\left(\frac{1}{r}\frac{\partial \psi}{\partial r}\right), \text{ on } \Gamma_1. \tag{14}$$

In order to satisfy these conditions, the length L_1 has to be sufficiently larger than R_1.

Conditions of no-slipping of the fluid on the walls Γ_2 and Γ_4, and incompressibility give the following relation:

$$\Omega = -\frac{1}{r}\frac{\partial^2 \psi}{\partial r^2} \text{ on } \Gamma_2, \Gamma_4. \tag{15}$$

The same conditions are to be satisfied on the boundaries Γ_3 and Γ_5:

$$\Omega = -\frac{1}{r}\frac{\partial^2 \psi}{\partial x^2} \quad \text{on } \Gamma_3, \Gamma_5. \tag{16}$$

The value of the stream function is defined with an arbitrary constant. On the boundary Γ_2, as well as on Γ_3 and Γ_4 that form the same streamline, this constant is arbitrarily chosen to be equal to zero. We thus have:

$$\psi = 0 \text{ on } \Gamma_2, \Gamma_3, \Gamma_4. \tag{17}$$

The continuity of the velocities on the boundary Γ_5 leads to the following expression:

$$U_x = \frac{d\gamma}{dt} = U_p(t) \quad \text{on } \Gamma_5, \tag{18}$$

where U_p designates the velocity of the piston.

Since this speed is independent of r, by using the first relation $(12a)$ connecting the axial component of the fluid velocity to the function ψ, we have the condition:

$$\psi = \frac{1}{2} r^2 U_p + c(t) \text{ on } \Gamma_5. \tag{19}$$

where $c(t)$ is a function of time.

The continuity of the stream function allows to determine its form. In fact, by continuity, this function is null for all t at the intersection of Γ_4 and Γ_5. We then have:

$$c(t) = -\frac{R_2^2}{2} U_p. \tag{20}$$

Finally, the axial symmetry and the hypothesis of incompressibility lead to:

$$\Omega = 0 \quad \text{and} \quad \psi = c(t) \text{ on } \Gamma_6. \tag{21}$$

II.2.b — Initial conditions

Initial conditions of the problem should be chosen in such a way that the time delay associated with the transient phase must be as short as possible. Nevertheless, because the only useful information is the near equilibrium position of the piston, we take the following conditions:

$$\gamma(0) = \gamma_0, \quad \frac{d\gamma}{dt}(0) = 0, \quad \psi(x, r, 0) = 0, \quad \Omega(x, r, 0) = 0. \tag{22}$$

III — Numerical implementation

The equations that we have obtained describe an oscillating coupled system which is strongly non linear. The coupling of the equations is realized throughout the deformable envelope on which a damping force acts. This force depends on the velocity field of the flow. By contrast, the non linearities are due both to the non linear convection term of the equations describing the fluid dynamics and to the variation of the inertia of the fluid contained in the cavity. The later depends strongly on the position of the piston.

The solution of the system of the coupled equations, given by relations ($9a$) and (11) – (13) associated with the boundary and initial conditions given respectively by (14) – (21) and (22), is not easy to obtain, in particular, when looking for the regime following after the transient phase. Nevertheless, within the range of the parameters considered here, a solution was derived by applying the time-staggered scheme which allows to integrate separately the equations describing the structure and those of the fluid during each time step [see, *e.g.* Piperno *et al.* (1996)]. The fluid part is discretized by the finite difference method associated with an Arbitrary

Lagrangian Eulerian formulation [see, *e.g.* Hughes *et al.* (1981)] of the governing fluid dynamic equations and the structure part defining the piston's movement by a RUNGE-KUTTA method. For a given time step, the fluid velocity field is determined by using the spatial configuration obtained at the previous step. This solution enables us to calculate the damping force given in the dimensionless form (4). At the next time step, we compute the new position of the piston which determines the new domain $\mathcal{D}$ as well as the associated boundary conditions.

The coupling is actually characterized by a cycle of energy exchange between the fluid and the structure. These changes of energy are instantaneous. Displacement of the fluid-structure interface produces an immediate modification of the flow. Reciprocally, a variation of the pressure and shear stress of the fluid induces a variation of the forces acting on the structure, which modifies its movement. This coupling occurs at the interface between the fluid and the structure. Such an interaction cycle almost all underlies the numerical methods useful in the problem of fluid-structure interaction. The main idea is based on the development of time-staggered schemes for the two subsystems. Firstly, the structure and the associated boundary value problem is generally discretized, for example, by using a classical finite element method. However, in our problem, the structure dynamics is a single degree of freedom problem, *i.e.* the axial position of the piston, and the motion of the structure is reduced to an initial value problem. So, this moving structure must be integrated only in time. Accordigly, we have used a well-known time-integration method usually used for solving this type of problems. Secondly,

the fluid to be discretized is enclosed in a box, which is deformed by the motion of the piston. Then, the numerical simulation requires the use of moving grids, at least at the fluid domain boundaries. We have considered the ALE formulation of NAVIER-STOKES equations, *i.e.* a formulation with imbedded hybrid coordinates. Here we present a numerical method used to solve this system of equations.

III.1 — Numerical method used for the fluid

The method used is a combination of two numerical schemes, a second-order method for the solution of the POISSON equation of the stream function given by $(11b)$, and a second-order one for the calculation of the vorticity transport equation given by $(11a)$.

III.1.a — Mesh of the domain

In order to find the numerical solution of the problem of the flow dynamics, we constructed a structured mesh where the nodes are designated by (x_i, r_j), for $i = 1, N$ and $j = 1, M$. The intersection point of the boundaries Γ_2 and Γ_3 is indexed by (I_c, J_c). The spatial steps of discretization in the x and r directions are defined respectively by the relations:

$$h_1 = \frac{L_1}{(I_c - 1)}, \quad h_2(t) = \frac{(L_2 + \gamma)}{(N - I_c)}, \quad h_r = \frac{R_1}{(J_c - 1)}. \tag{23}$$

Thus, the coordinates of the mesh nodes in the domains $\mathcal{D}_1$ and $\mathcal{D}_2$ are given as indicated in figure 2 by the following relations:

$$x_i = h_1(i-1), i = 1, I_c \quad r_j = h_r(j-1), j = 1, J_c \quad \text{in } \mathcal{D}_1$$

$$x_i = L_1 + h_2(i - I_c), i = I_c, N \quad r_j = h_r(j-1), j = 1, M \quad \text{in } \mathcal{D}_2.$$

III.1.b — Solution of POISSON's equation with the stream function

The 2nd spatial derivatives of ψ at the point (x_i, r_j) are approximated as follows:

$$\left\{ \frac{\partial}{\partial r}\left(\frac{1}{r}\frac{\partial \psi}{\partial r}\right) \right\}_{ij} = \frac{1}{h_r^2}\left\{ \frac{\psi_{ij+1} - \psi_{ij}}{(r_j + h_r/2)} + \frac{\psi_{ij} - \psi_{ij-1}}{(r_j - h_r/2)} \right\} + O(h_r^2), \tag{24a}$$

$$\left\{ \frac{\partial^2 \psi}{\partial x^2} \right\}_{ij} = \frac{1}{h_k^2}\left\{ \psi_{i+1j} - 2\psi_{ij} + \psi_{i-1j} \right\} + O(h_k^2), \quad k = 1, 2. \tag{24b}$$

The method of implicit relaxation is chosen for the calculation of POISSON's equation [see, *e.g.* Roache (1982)]. The finite difference equation obtained by discretization of the equation (11b) is solved by a technique derived from the generalized Alternating Direction Method scheme, noted ADI [see, *e.g.* Roache (1982)].

In equation (11b) only ψ and its second derivatives appear. So, by using relations (24a) and (24b) we can write for each step of the $(m+1)$th iteration of the ADI technique :

$$\frac{1}{\lambda}\psi_{ij}^{m+1/2} - \frac{1}{r_j}\left\{ \frac{\partial^2 \psi}{\partial x^2} \right\}_{ij}^{m+1/2} = \Omega_{ij}^{n+1} + \left\{ \frac{\partial}{\partial r}\left(\frac{1}{r}\frac{\partial \psi}{\partial r}\right) \right\}_{ij}^{m} + \frac{1}{\lambda}\psi_{ij}^{m}, \tag{25a}$$

and

$$\frac{1}{\lambda}\psi_{ij}^{m+1} - \left\{ \frac{\partial}{\partial r}\left(\frac{1}{r}\frac{\partial \psi}{\partial r}\right) \right\}_{ij}^{m+1} = \Omega_{ij}^{n+1} + \frac{1}{r_j}\left\{ \frac{\partial^2 \psi}{\partial x^2} \right\}_{ij}^{m+1/2} + \frac{1}{\lambda}\psi_{ij}^{m+1/2}, \tag{25b}$$

where λ is the relaxation coefficient and n is the index of the time step.

For each line (i) or (j), the tridiagonal system obtained is solved by the factorization algorithm [see, *e.g.* Roache (1982)].

The initial values of ψ for the iterative procedure are taken equal to ψ^n.

The scheme given by equation $(25a)$ is applied successively on each of the domains $\mathcal{D}_1$ and $\mathcal{D}_2$. The boundary conditions on the interface between $\mathcal{D}_1$ and $\mathcal{D}_2$ has been calculated by the quadratic interpolation on each iteration. The same procedure is applied to the equation $(25b)$.

III.1.c — Solution of the vorticity transport equation

A scheme that is accurate to second-order has been chosen to solve the equation $(11a)$. Besides to being easy to implement this scheme allows a simple check of the boundary conditions and by use of the second order upwind approximation of the transport terms.

As for the treatment of the POISSON stream function equation, the generalized ADI algorithm has been used for the vorticity transport equation [see, *e.g.* Roache (1982)]. Each dimensionless time step Δt is decomposed into two successive half steps with first order accuracy. n being index of the nth time step, we have the following expressions:

$$\frac{1}{\Delta t/2}\Omega_{ij}^{n+1/2} + \left\{\frac{\partial(\Omega^{n+1/2}V_x^n)}{\partial x}\right\}_{ij} + \left\{\frac{\partial(\Omega^n V_r^n)}{\partial r}\right\}_{ij} - \left\{\frac{\partial W_x^n}{\partial x}\frac{\partial U_x^n}{\partial r}\right\}_{ij} + \left\{\frac{\partial W_r^n}{\partial r}\frac{\partial U_r^n}{\partial r}\right\}_{ij} - \left\{\frac{\partial W_r^n}{\partial x}\frac{\partial U_r^n}{\partial r}\right\}_{ij} + \left\{\frac{\partial W_x^n}{\partial x}\frac{\partial U_x^n}{\partial x}\right\}_{ij} = \frac{1}{\alpha^2}\left[\left\{\frac{\partial^2\Omega^{n+1/2}}{\partial x^2}\right\}_{ij} + \left\{\frac{\partial}{\partial r}\left(\frac{1}{r}\frac{\partial(r\Omega^n)}{\partial r}\right)\right\}_{ij}\right] + \frac{1}{\Delta t/2}\Omega_{ij}^n, \qquad (26a)$$

and

$$\frac{1}{\Delta t/2}\Omega_{ij}^{n+1} + \left\{\frac{\partial(\Omega^{n+1/2}V^n)}{\partial x}\right\}_{ij} + \left\{\frac{\partial(\Omega^{n+1}V^n)}{\partial r}\right\}_{ij} - \left\{\frac{\partial W_x^n}{\partial x}\frac{\partial U_x^n}{\partial r}\right\}_{ij} + \left\{\frac{\partial W_r^n}{\partial r}\frac{\partial U_r^n}{\partial r}\right\}_{ij} - \left\{\frac{\partial W_r^n}{\partial x}\frac{\partial U_r^n}{\partial r}\right\}_{ij} + \left\{\frac{\partial W_x^n}{\partial x}\frac{\partial U_x^n}{\partial x}\right\}_{ij} =$$
$$\frac{1}{\alpha^2}\left[\left\{\frac{\partial^2\Omega^{n+1/2}}{\partial x^2}\right\}_{ij} + \left\{\frac{\partial}{\partial r}\left(\frac{1}{r}\frac{\partial(r\Omega^{n+1})}{\partial r}\right)\right\}_{ij}\right] + \frac{1}{\Delta t/2}\Omega_{ij}^{n+1/2}, \qquad (26b)$$

where the discretized analogues of the spatial derivatives in (26a) and (26b) are expressed by the following terms:

$$\left\{\frac{\partial(\Omega V_x)}{\partial x}\right\}_{ij} = \frac{1}{2h_k}\left\{(V_x^+ - \mid V_x^+ \mid)\Omega_{i+1j} - (V_x^- + \mid V_x^- \mid)\Omega_{i-1j} + (V_x^+ + \mid V_x^+ \mid - V_x^- + \mid V_x^- \mid)\Omega_{ij}\right\}, \quad k = 1, 2 \qquad (27a)$$

$$\left\{\frac{\partial(\Omega V_r)}{\partial r}\right\}_{ij} = \frac{1}{2h_r}\left\{(V_r^+ - \mid V_r^+ \mid)\Omega_{ij+1} - (V_r^- + \mid V_r^- \mid)\Omega_{ij-1} + (V_r^+ + \mid V_r^+ \mid - V_r^- + \mid V_r^- \mid)\Omega_{ij}\right\}, \qquad (27b)$$

$$\left\{\frac{\partial}{\partial r}\left(\frac{1}{r}\frac{\partial(r\Omega)}{\partial r}\right)\right\}_{ij} = \frac{1}{h_r^2}\left\{2\frac{(r_j + h_r)}{(2r_j + h_r)}\Omega_{ij+1} - \frac{8r_j^2}{(2r_j + h_r)}\Omega_{ij} + 2\frac{(h_r - r_j)}{(2r_j - h_r)}\Omega_{ij-1}\right\}, \qquad (27c)$$

where V_x^+, V_x^-, V_r^+ and V_r^- are difference operators defined by:

$$V_x^+ = \frac{1}{4r_j h_r}\left\{\psi_{ij+1} - \psi_{ij-1} + \psi_{i+1j+1} - \psi_{i+1j-1}\right\} - \frac{1}{2}\left\{\left(W_x\right)_{ij} + \left(W_x\right)_{i+1j}\right\}$$

$$V_x^- = \frac{1}{4r_j h_r}\left\{\psi_{ij+1} - \psi_{ij-1} + \psi_{i-1j+1} - \psi_{i-1j-1}\right\} - \frac{1}{2}\left\{\left(W_x\right)_{ij} + \left(W_x\right)_{i-1j}\right\}$$

$$V_r^+ = \frac{1}{4r_j h_k}\left\{\psi_{i+1j} - \psi_{i-1j} + \frac{1}{(r_j + h_r)}(\psi_{i+1j+1} - \psi_{i-1j+1})\right\} - \frac{1}{2}\left\{\left(W_r\right)_{ij} + \left(W_r\right)_{ij+1}\right\}, \quad k = 1, 2$$

$$V_r^- = \frac{1}{4r_j h_k}\left\{\psi_{i+1j} - \psi_{i-1j} + \frac{1}{(r_j - h_r)}(\psi_{i+1j-1} - \psi_{i-1j-1})\right\} - \frac{1}{2}\left\{(W_r)_{ij} + (W_r)_{ij-1}\right\}, \quad k = 1, 2.$$

All of the other derivatives of the equation $(11a)$ have been discretized by the central difference of the second order accuracy. The total order of accuracy of this scheme is $O(h_k^2, h_r^2, \Delta t)$.

The tridiagonal system obtained from the equations $(26a)$ and $(26b)$ is also solved by using the factorization algorithm.

The same procedure as that for POISSON's equation is used on the interface between the domains $\mathcal{D}_1$ and $\mathcal{D}_2$.

III.1.d — Boundary conditions

Boundary conditions are very simple since ψ is known everywhere at the boundary of the domain $\mathcal{D}$ and its second derivatives can be expressed in terms of the vorticity function by equations $(14), (15), (16)$ and (18). So, the vorticity on the wall is obtained by applying the no-slip condition. Regardless of the wall orientation or the boundary value of ψ, we can write :

$$\Omega_w = \frac{-7\psi_w + \psi_{w+1} - \psi_{w+2}}{2\Delta w^2} + O(\Delta w^2), \tag{28}$$

where Δw is the distance between $(w + 1)$ and w, normal to the wall and the index w corresponds to the wall. The above frequent form was first used by Jensen (1959).

III.2 — Numerical method used for the structure

In the model considered here, the dynamics of the structure part is particularly simple because it is described by a system with only one degree of freedom. The motion of the structure defined from the axial position of the piston is reduced to an initial value problem. This problem is gouverned by equation ($9a$) and the first two initial conditions are given by (22). For the solution of equation ($9a$), we use an accurate RUNGE-KUTTA method of fourth order in time. In the RUNGE-KUTTA method the second order differential equation is reduced to two first order equations [see, *e.g.* Boyce & Diprima (1986)].

III.3 — Numerical strategy for the coupling

In this part, we deal with the numerical methods which are needed for the simulation of the coupled fluid and structure fields. We have presented in the two previous sections a method for the simulation of the dynamics on a motion of the domain relative to the deformable structure and the fluid considered as decoupled systems. The goal of this section is to introduce a method that deals with model the coupling phenomenon.

We consider time-staggered strategies: they consist of successive decoupled integrations of the structure and fluid dynamics equations. Each field is frozen during the integration time of the other one. This kind of strategy has many advantages. First, the use of existing schemes, numerical codes and procedures for both separate fields is made possible. Second, the use of implicit schemes in a totally coupled time integration scheme would induce a prohibitive computational cost, because the grid position and velocity would be considered as numerical

variables as well. On the other hand, this kind of time-staggered scheme may not be stable, even if both schemes used for separate fields are used far below stability limits.

The basic line of a time-staggered algorithm can be sketched as follows :

a — assume that all quantities after the nth time step are known. There are not only the structural elongation and fluid velocities but also the locations and velocities of all fluid grid points. We shall denote these quantities by S^n – structural –, M^n – fluid mesh – and F^n – fluid field – at nth time step.

b — compute the damping force, due to the viscous effects exerted by the fluid on the structure.

c — assume this term as constant during the next time step and calculate the state of the structure one step later to get S^{n+1}.

d — compute a possible fluid grid after the current time-step. The future grid M^{n+1} must satisfy the condition that both the fluid and the structural boundaries should match along the interface at time t^{n+1}.

e — compute the distribution of each fluid grid speed points during the current time step.

f — use the new fluid grid and its speed field for the time integration of the fluid and get F^{n+1}.

The preceeding algorithm is applicable to many physical systems because of its versatility [see, *e.g.* Shankar & Ide (1988)].

As already underlined, the ALE description has been developed because it

succeeds, to a certain extent, in combining the best features of both the Lagrangian and Eulerian approaches. The advantage offered by the ALE formulation in its ability to move the grid independently of the material points, could disappear completely if the task to determine the optimal speed of the grid were to be manual. In other terms, the success of the method lies in its capacity to prescribe automatically the movement of the grid step by step in the course of the calculation. Unfortunately, none of the automatic mesh rezoning algorithm available to date guarantees efficiency in general conditions. For example, * the algorithm developed by Giuliani (1982) uses a purely geometrical criterion to overcome this difficulty. In our case, the used criterion aims at minimizing the dilation of the elements. Therefore, in ordre to guarantee the convergence of the numerical scheme, especially in the exceptional conditions of very large cavity deformations, in which the mesh aspect ratio becomes incompatible with the defined choices, we imposed the following condition:

$$\text{If } \bar{\gamma} \leq -\frac{1}{2}\bar{L}_2 \text{ then } \bar{\gamma} = -\frac{1}{2}\bar{L}_2 \text{ and } \bar{U}_p = 0. \tag{29}$$

III.4 — Validation of the numerical scheme

To validate the numerical scheme we have carried out a certain number of tests. In particular, a study has been conducted of the sensitivity to the mesh size. A number of solutions with different grid sizes have been carried out to test the rate of convergence of the solution. We have checked the grid sensitivity of the scheme by dividing by two the space steps $h_1, h_2(t)$ and h_r. No noticeable

difference has been obtained for this type of tests. The time sensitivity of the scheme was tested similarly. When the time step Δt is divided by two, we do not observe any significant difference in accuracy (see section III.1.c and III.2) of the results or the convergence towards a periodic regime. Numerical tests have also been carried out under conditions of excitation loading and damping that one obtains small elongations of the spring. These tests allow to establish the conditions in which the system behaves linearly. The motion of the piston is that of a harmonic oscillator.

IV — Results and discussion

IV.1 — General case

The values of the geometrical parameters of the system are chosen in accordance with the experimental model designed by Dantan (1985) in a physical simulation of the cardiac hemodynamics. Thus, we deduced the following values :

$$\bar{L}_1 = \bar{L}_2 = 0.42, \quad \bar{R}_2 = 0.27, \quad D_r = 0.25, \quad S = 0.15, \tag{30}$$

in accordance with $R_1 = 0.01m, R_2 = 0.026m$ and $L_1 = L_2 = 0.04m$. With these geometrical data, we obtain the parameter $\bar{\gamma}_0$ which is linked to the parameter D_r according to the first relation $(10b)$.

In the range of values considered here and after a transient phase, the numerical results show that the system response as characterized by the displacement of the piston has a period close to the excitation one. The periodic and vortical regime of the flow induces a periodic and anharmonic motion of the piston as shown below.

In figure 3, we give an example describing the streamlines of the fluid during one period. The characteristics that we have used are $P_a = 38, \alpha = 250$ and $K = 14$. They correspond to an average values of experimental data obtained by Abe *et al.* (1981) on the cardiac hemodynamics. The period represented on this figure corresponds to a reduced interval time of the order of 2π. This interval defines the oscillation periods of the piston, whose motion is related to that of the fluid. Figure $3a$ shows the system when the position of the piston is minimal. We observe the presence of three vortices inside the cavity. This state is due to the reverse in the direction of the velocity of the piston. Inflow is illustrated in figures $3b$ to $3g$. Figure $3g$ corresponds to the maximal position of the piston. It is obvious from the examination of figures $3a - 3g$ that the vortex is generated at the inlet, convected and grown by diffusion within the cavity. Ultimately the vortex occupies the whole cavity. It should be pointed out that the propagation velocity of this vortex is greater than that of the piston. The outflow is shown in figures $3h$ to $3l$. At that stage, the vortex propagates towards the axis of symmetry and its extent decreases. We verify through figure $3a$ and $3m$ that the periodic regime of the piston's movement is also valid for the fluid flow. Since the amplitudes of the piston normalized displacement can be significant, *i.e.* close to 0.8, the amount of fluid contained in the cavity also varies strongly. This quantity is a linear function associated with the amplitude and is defined in its dimensionless form by the relation: $\pi(\bar{R}_1^2\bar{L}_1 + \bar{R}_2^2\bar{L}_2 + \bar{R}_2^2\bar{\gamma})$. A significant increase in this quantity is able to induce important non linear effects seen below.

In such a dynamical system, the two most influent parameters are the structure rigidity and the fluid viscosity. To characterize the behavior of the system, we introduce the amplitude A of the normalized piston elongation $\bar{\gamma}$, defined by the relation $A = \bar{\gamma}_M - \bar{\gamma}_m$, where $\bar{\gamma}_M$ and $\bar{\gamma}_m$ designate respectively the maximal and minimal values of $\bar{\gamma}(\bar{t})$ in the periodic regime.

We show in figure 4 the evolution of A *versus* K when $P_a = 1$ for four values of α which quantify the influence of viscous effects in the response of the system. They clearly show that an important increase in A occurs for $K \sim 1$. This corresponds to the resonance. This expresses the well known fact that the viscosity effects tend to decrease the amplitude of $\bar{\gamma}$ at resonance. On the other hand, we notice an important dependence of A on α for $0.3 \leq K \leq 3.0$. In fact, when α increases, we observe that the maximum of A is displaced to the left, revealing a change in resonant frequency with the viscous effect. Moreover as is well known with such a system we notice also under the same conditions an increase in the width of the resonance curve. Furthermore, above a threshold in piston displacement non linear effects generate an asymmetry in the response.

These results can be analyzed by dynamical system methods, particularly in plotting the phase portrait of a system of partial differential equations. In figure 5, we give an example of the phase plane $\dot{\bar{\gamma}}$ *versus* $\bar{\gamma}$ for the values of the parameters used in figure 3. This plot shows the stable limit cycle of the system and the relaxation of the motion of the piston. Thus, this figure clearly shows the periodic and anharmonic regime of the piston response characterized by a limit cycle which

is a non elliptic closed trajectory. It is useful to compare this result with figure 6 where we give the dependence $\dot{\bar{\gamma}}$ *versus* $\bar{p}_s$, where $\bar{p}_s = P_a \sin(\bar{t} - \pi/2)$, which has almost the same angle to the abscissa axis and nearly the same form of the stable limit cycle as that in figure 5. This means that our system is almost linear for the choice of the parameter used for this calculation and this because the frequency, the form and the phase differences between the excitation pressure and the forced oscillation are nearly the same.

Now, we explicit the way and the conditions under which the system equations can be decoupled. To this end, we need to give an approximation of the term $\bar{f}_f$ that is independent of the fluid velocity field. To do so, we use the conservation of the flow rate and we approximate the gradient of the velocity in the radial direction by the ratio between the average speed of the cross section and its associated radius. This approximation results into a parabolic profile of the fluid velocities that determines the gradient of the velocities at the wall. This gradient is linked to the speed of the piston for each cross section of the domains $\mathcal{D}_1$ and $\mathcal{D}_2$. Finally, the equation $(9a)$ can be approximated by the following expression:

$$\frac{d}{d\bar{t}}\left\{(\bar{L}_1 + \bar{L}_2 + \bar{\gamma}(\bar{t}))\frac{d\bar{\gamma}}{d\bar{t}}\right\} + \frac{1}{\pi \bar{R}_2^2 \alpha^2}\frac{d\bar{\gamma}}{d\bar{t}}\left\{\frac{\bar{L}_1}{S} + \bar{L}_2 + \bar{\gamma}\right\} + K(\bar{\gamma} - \bar{\gamma}_0) = SP_a \sin(\bar{t} - \pi/2). \tag{31}$$

The choice of the type of velocity profile which best approximates such an unsteady flow inside a cavity is a real problem: taking into account that vortical patterns within the flow field are observed in the vicinity of this type of geometrical

singularity, due to the sudden expansion of the tube, it is difficult to assume any realistic profile under unsteady conditions. Nevertheless, considering only the case of unsteady developed flow inside a straight tube, a WOMERSLEY profile would be convenient. Such a profile can be approached by a POISEUILLE or blunt profile depending on whether $\alpha \lesssim 1$ or $\alpha \gg 1$ respectively. Owing to the way the parameter has been defined here — the characteristic length which allows to define α is the length of the system, whereas it is traditionally defined with the radius of the tube — we are very close to the first case for the different values which have been tested and so an instantaneous parabolic profile seems a reasonable approach.

This approximation has the merit to simplify considerably the problem and to reproduce faithfully enough the behavior of the coupled system as shown in figure 7, for all A. The values of the characteristic parameters of the system of figure 7 are identical to those of figure 4. We also notice a sharp break of the slope of the curve for α equals 20 and 100 when the system is in resonance. These slope breaks are due to the conditions given by relation (29).

We show now in figure 8 the evolution of A *versus* P_a for three values of α when $K = 10$, *i.e.* we suppose that inertia effects are negligible compared to the deformation capacity effects of the system. They reveal a slight influence of the dissipative effects on A in the interval $[10, 50]$ of P_a. These effects can be explained by the presence of vortices in the fluid. The analysis of the order magnitude indicates that vortices have a significant influence only when K is of the same order of magnitude as P_a.

Now by exploiting the approximation given by the relation (31) and by using the same data as these of figure 8, we observe in figure 9 that the curves show a qualitatively similar overall behavior without the vortices in the fluid. The angle change of the curves shown in figures 8 and 9 can be explained by the role of the limiting condition (29). In fact, the formation and propagation process of the fluid vortices are not taken into account by the above approximation. By comparing the results shown in figures 8 and 9 we notice the importance of these processes on the dynamical behavior of the system in the range $P_a \in [10.0, 50.0]$.

IV.2 — Small elongation case

The local behavior of the non linear equation (31), associated with the initial conditions given by the first two equations (22), near an equilibrium state is qualitatively determined by the behavior of the linear equation. The linearization of this equation is obtained for small movements $(\bar{\gamma} - \bar{\gamma}_0)$, since in that case the convection effects of the fluid are negligible and the inertia of the system depends weakly on the slight elongation of the spring.

Letting $v = \bar{\gamma} - \bar{\gamma}_0$ and $u = \dfrac{dv}{d\bar{t}}$, we give the corresponding autonomous system for the small motion :

$$\begin{cases} \dfrac{dv}{d\bar{t}} &= u \\ \dfrac{du}{d\bar{t}} &= -bu^2 - cu - dv \end{cases} \tag{32}$$

where

$$b = \frac{1}{\bar{L}_1 + \bar{L}_2 + \bar{\gamma}_0}, \quad c = \frac{\frac{\bar{L}_1}{\bar{S}} + \bar{L}_2 + \bar{\gamma}_0}{\pi \bar{R}_2^2 \alpha^2 (\bar{L}_1 + \bar{L}_2 + \bar{\gamma}_0)}, \quad d = \frac{K}{\bar{L}_1 + \bar{L}_2 + \bar{\gamma}_0}.$$

The point $(u, v) = (0, 0)$ is a critical point of the system (32). Because of the

damping mechanism, we expect any small motion $\bar{\gamma} = \bar{\gamma}_0$ to decay in amplitude. Intuitively we thus expect the equilibrium point $(0, 0)$ to be asymptotically stable. To show this, we neglect the non linear term in the system (32), so the eigenvalues of the corresponding linear system are:

$$\lambda_{1,2} = \frac{-c \pm \sqrt{c^2 - 4d}}{2}.$$

Three different cases follow:

— if $c^2 - 4d > 0$ the eigenvalues are real, unequal, and negative. The critical point $(0, 0)$ is an asymptotically stable improper node of the system,

— if $c^2 - 4d = 0$ the eigenvalues are real, equal, and negative. The critical point $(0, 0)$ is an asymptotically stable node of the system (32). It may be either an asymptotically stable node or an asymptotically stable spiral point of the system,

— if $c^2 - 4d < 0$ the eigenvalues are complex with negative real parts. The critical point $(0, 0)$ is an asymptotically stable spiral point of the system.

Thus, the critical point $(0, 0)$ is the stable point for all choices of the system parameters, *i.e.* the system is an equilibrium state given by the position $\bar{\gamma} = \bar{\gamma}_0$ with a zero piston speed.

V — Conclusion

In this paper, a complex problem of fluid-wall interaction has been studied in detail. The proposed model reports not only on the large movements of the wall but also on the variation of the mass system. The fluid dynamics is expressed in

a vorticity-stream function formalism associated with an Arbitrary Lagrangian Eulerian description. In this formulation, the forces acting on the system are given and the unknowns are essentially kinematics. Subsequently, we have shown that five characteristic dimensionless parameters are relevant for analyzing the mechanical behavior of the system. The system of the coupled equations has then been solved by applying a time-staggered scheme. Processes of creation, development and propagation of the vortices within the fluid dynamics inside the cavity have been emphasized. The non linear dynamical behavior of the system was illustrated by using the phase portrait method. We have shown that the system displays a stable limit cycle. The response can be characterized as being both periodic and anharmonic, with a fundamental period equal to the excitation. In addition, the characteristic curves of resonance are analyzed when varying the WOMERSLEY's parameter. In order to decouple the system of the equations, an approximation of the damping force was proposed, based upon the assumption of a POISEUILLE approximation of the velocity profile within the cavity. The conditions required to obtain such a result were analyzed from the characteristic resonance curves. The case of small piston displacement was obtained by linearization and an analysis of the system stability was given.

References

Abe H., Nakamura T., Kimura T., Motomiya M., Konno K., Arai S. & Suzuki N. 1981 Stress-strain relation of cardiac muscle determined from ventricular pressure-time relationship during isovolumetric contractions. Journal of Biomechanics, **14**, No. 5, p. 357-360.

Boederick L.L. & Leonard J.W. 1995 Nonlinear response of membranes to ocean waves using boundary and finite elements. Ocean Engineering, **22**, p. 731-745.

Boyce W. E., Diprima R.C. 1986 *Elementary differential equations and boundary value problems*. New York: John Wiley & Sons.

Dantan P. 1985 *Etude numérique et expérimentale de l'écoulement instationnaire d'un fluide visqueux incompressible dans une cavité de dimension variable. Modélisation de l'hémodynamique cardiaque*. PhD thesis, Université Paris 7.

Delemarre B.J., Bot H., Pearlman A.S., Visser C.A.& Dunning A.J. 1987 Diastolic flow characteristics of severely impaired left ventricles: a pulsed Doppler ultra-sound study. J. Clin. Ultrasound, **15**, p. 115-119.

Giuliani S. 1982 An algorithm for continuous rezoning of the hydrodynamic grid in arbitrary Lagrangian-Eulerian computer codes. Nuclear Engineering and Design, **72**, p. 205-212.

Guruswamy G.P. 1988 Interaction of fluids and structures for aircraft applications. Computers & Structures, **30**, No. 1/2, p. 1-13.

Guyon E., Hulin J.P. & Petit L. 1991 *Hydrodynamique physique*. InterEdi-

tions.

Heil M. 1998 Stokes flow in an elastic tube — A large-displacement fluid-structure interaction problem. International Journal for Numerical Methods in Fluids, **28**, p. 243-265.

Hughes T.J.R., Liu W.K., Zimmermann T.K. 1981 Lagrangian-Eulerian finite element formulation for incompressible viscous flows. Computer Methods in Applied Mechanics and Engineering, **33**, p. 329-349.

Jensen V.G. 1959 Viscous flow round a sphere at low Reynolds number. Proceeding of the Royal Society of London, Series A, **249**, p. 346-366.

Piperno S., Larrouturou B., Lesoinne M. 1996 Analysis and compensation of numerical damping in a one-dimensional aeroelastic problem. Int. J. Comput. Fluid Dynamics, **6**, p. 157-174.

Roache P.J. 1982 *Computational fluid dynamics*. Albuquerque: Hermosa publishers.

Shankar V., Ide I. 1988 Aeroelastic computations of flexible configurations. Computers & Structures, **30**, No. 1/2, p. 15-28.

Legends of the figures

Fig. 1

Diagrammatic representation of the studied system. Γ_1 designates the entry and exit sections of the system, $\Gamma_2, \Gamma_3, \Gamma_4$ represent the lateral fixed walls, Γ_5 designates the surface of the rigid piston, Γ_6 is the axis of symmetry, γ is the elongation of the spring, R_1, R_2, L_1, L_2 are respectively the radii and lengths of the cavity, x, r, θ designate the cylindrical coordinates, $\mathcal{D}_1, \mathcal{D}_2$ represent the domains containing the fluid and $\mathbf{B}_T$ represents a fixed frame supporting the envelope.

Fig. 2

Mesh of the domain. The indices i, j represent the numbers of mesh nodes in the x and r directions respectively, h_1, h_2, h_r are the spatial steps of discretization. The intersection point of the boundaries Γ_2 and Γ_3 are indexed by (I_c, J_c).

Fig. 3

Flow streamlines during one period. The characteristics used are $P_a = 38, \alpha = 250$ and $K = 14$. (a) the system where the piston is at its minimal position. $(b)-(e)$ the system in the phase of inflow, where (e) describes the system where the piston is at its maximal position. $(f) - (h)$ the system in the phase of outflow. (i) the movement of the fluid is at the periodic regime.

Fig. 4

Variation of A *versus* K for values of $\alpha = 5, 10, 20$ and 100 when $P_a = 1$. Notice the sharp breaks of the curve's slope for α equals 20 and 100 when the system is close to the resonance state. These slope breaks are due to the conditions given

by relation (29).

Fig. 5

Example of the phase diagram $\dot{\bar{\gamma}}$ *versus* $\bar{\gamma}$ for same values of the parameters as the one presented in figure 3. It displays a limit cycle which is asymptotically stable.

Fig. 6

Example of the phase diagram $\dot{\bar{\gamma}}$ *versus* $\bar{p}_s$, where $\bar{p}_s = P_a \sin(\bar{t} - \pi/2)$ — same parameter values as in figure 3.

Fig. 7

Variation of A *versus* K when is used the approximation given by the relation (31) — same parameter values as in figure 4.

Fig. 8

Variation of A *versus* P_a for values of $\alpha = 10, 20$ and 100 when $K = 10$.

Fig. 9

Variation of A *versus* P_a when is used the approximation given by the relation (31) — same parameter values as in figure 8 .

Figure 1

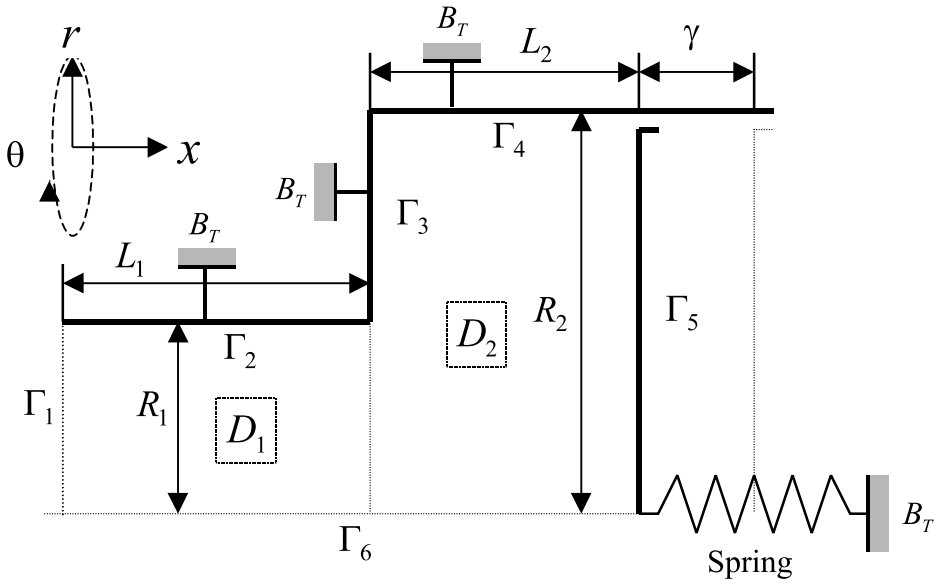
r
θ
x
B_T
L_2
γ
Γ_4
B_T
Γ_3
B_T
L_1
Γ_2
D_2
R_2
Γ_5
Γ_1
R_1
D_1
Γ_6
B_T
Spring

Figure 2

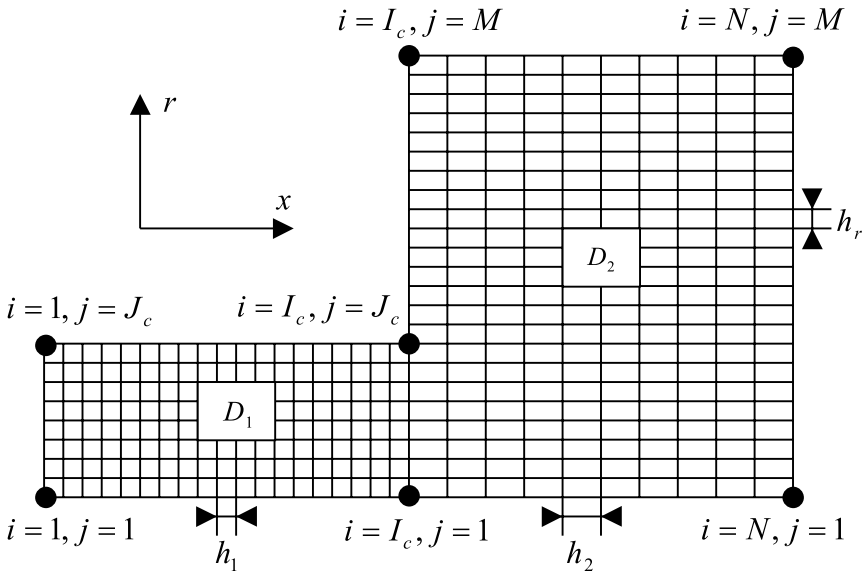

Figure $3a$

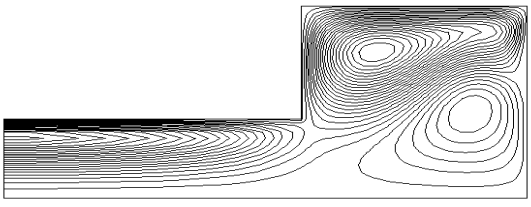

Figure 3*b*

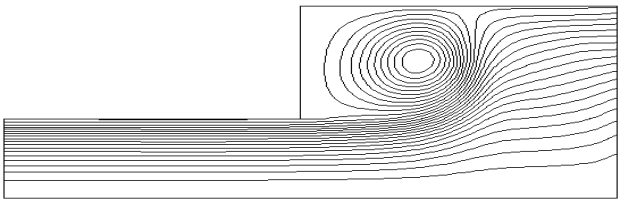

Figure 3*c*

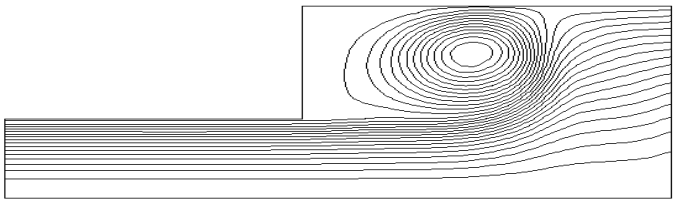

Figure $3d$

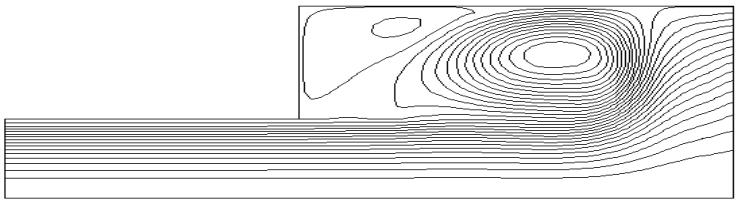

Figure 3*e*

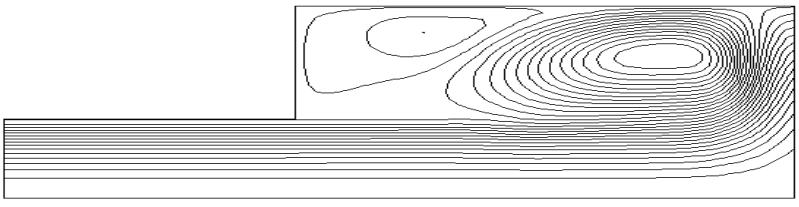

Figure $3f$

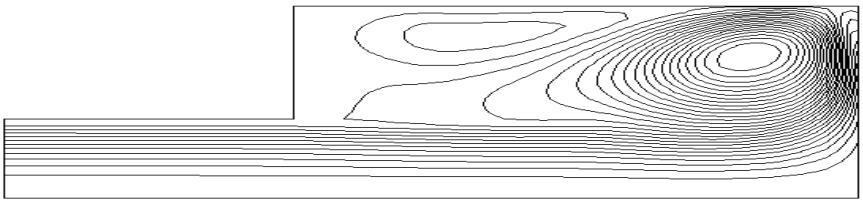

Figure $3g$

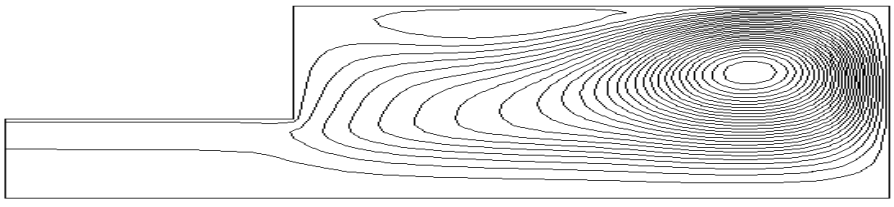

Figure $3h$

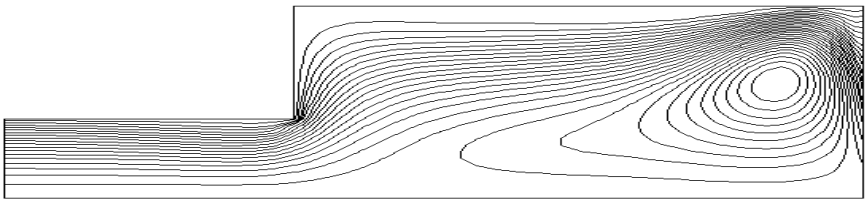

Figure $3i$

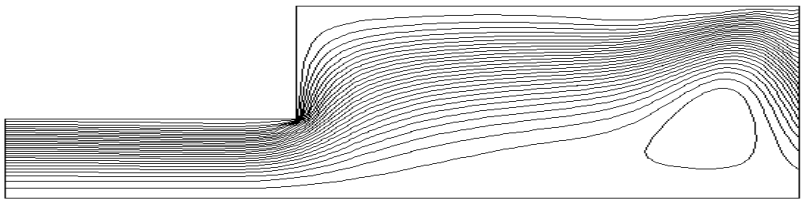

Figure $3j$

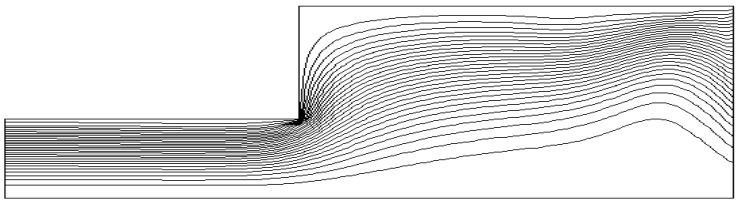

Figure $3k$

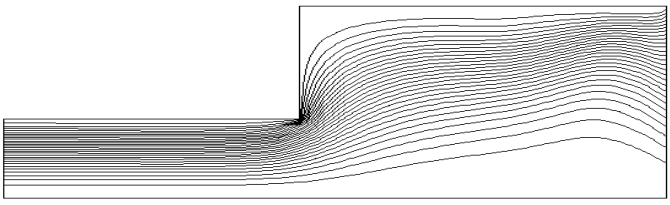

Figure $3l$

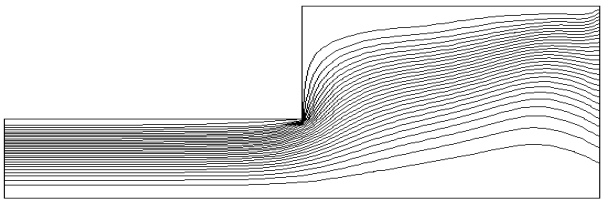

Figure $3m$

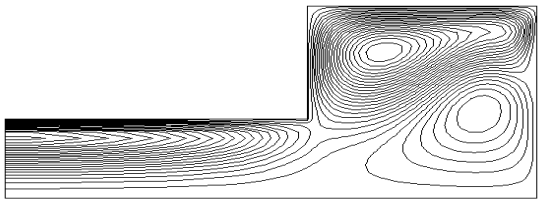

Figure 4

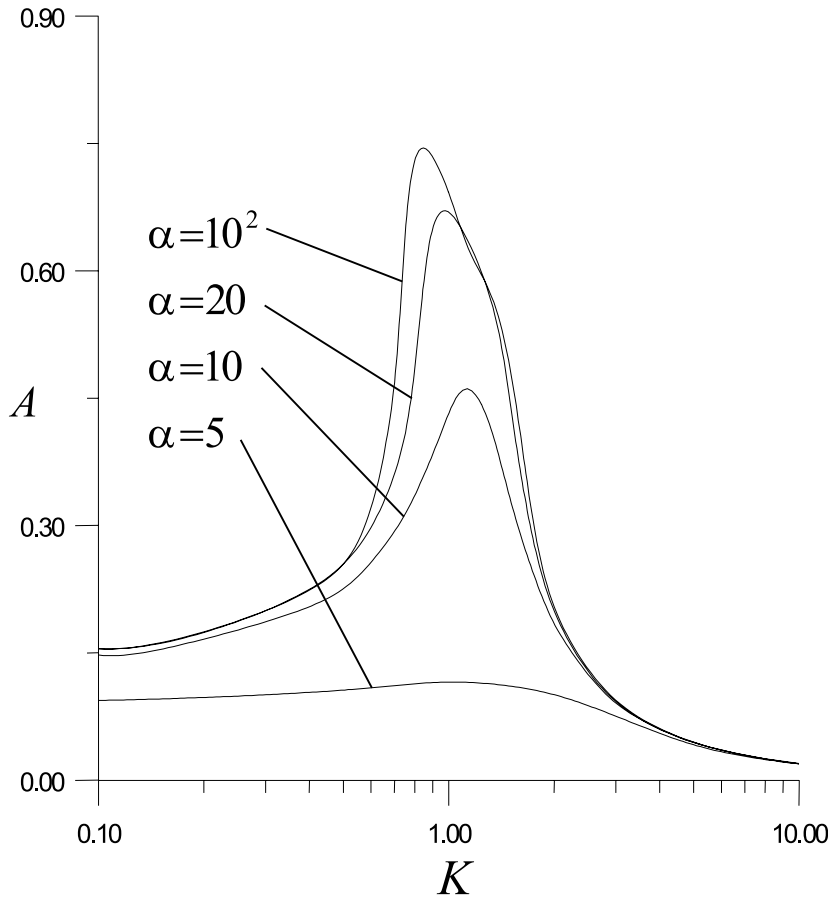

Figure 5

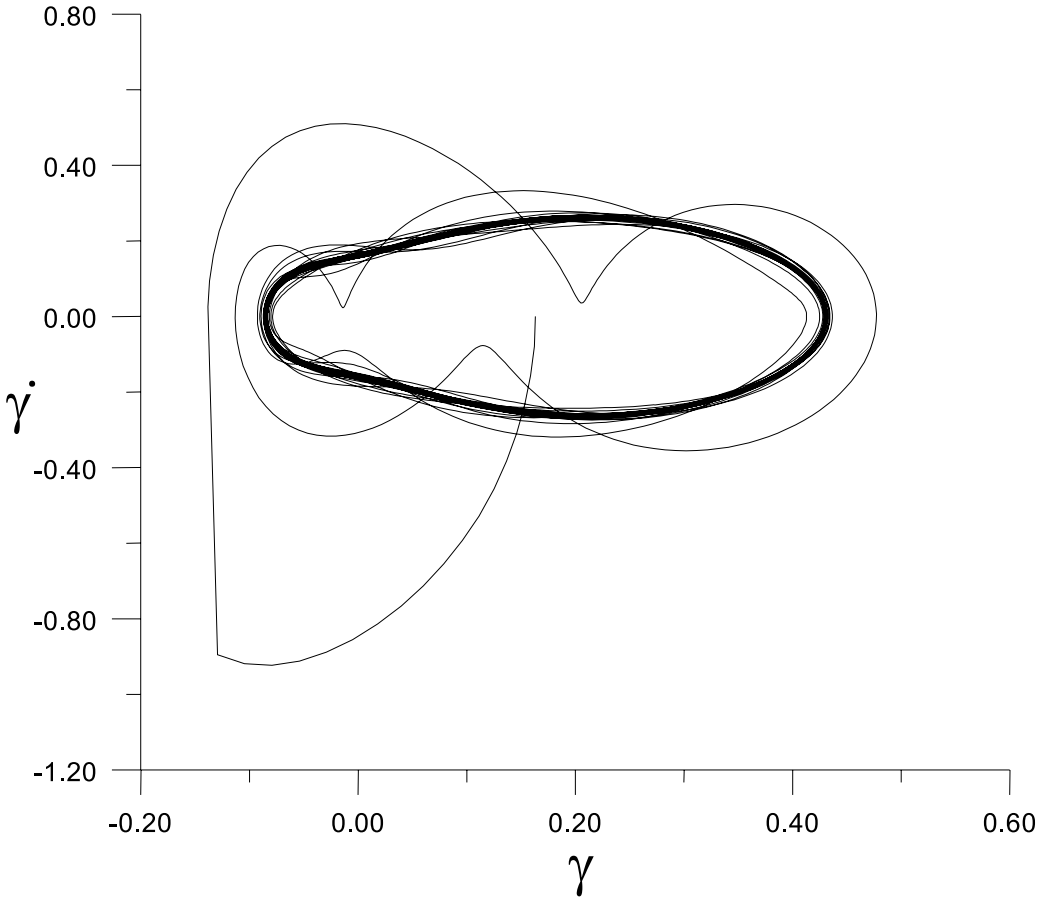

Figure 6

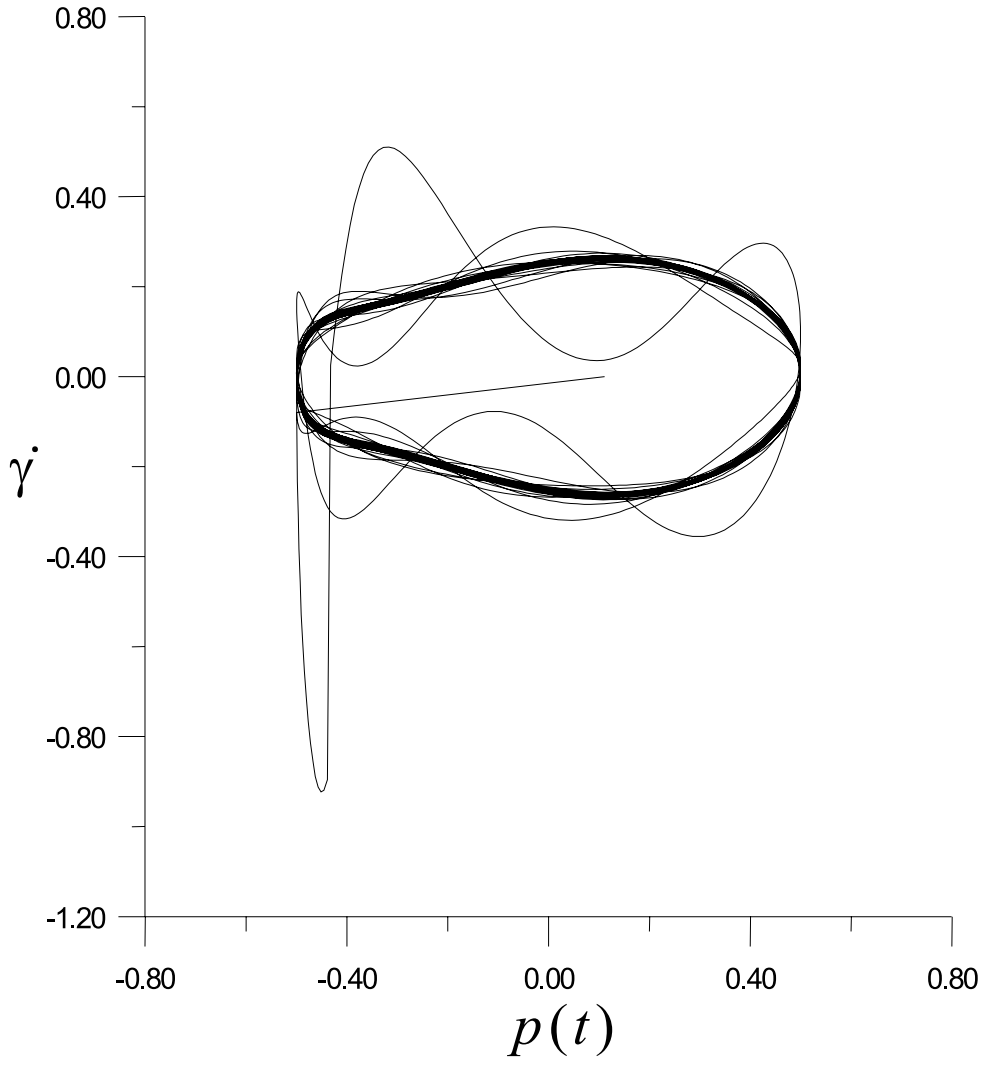

Figure 7

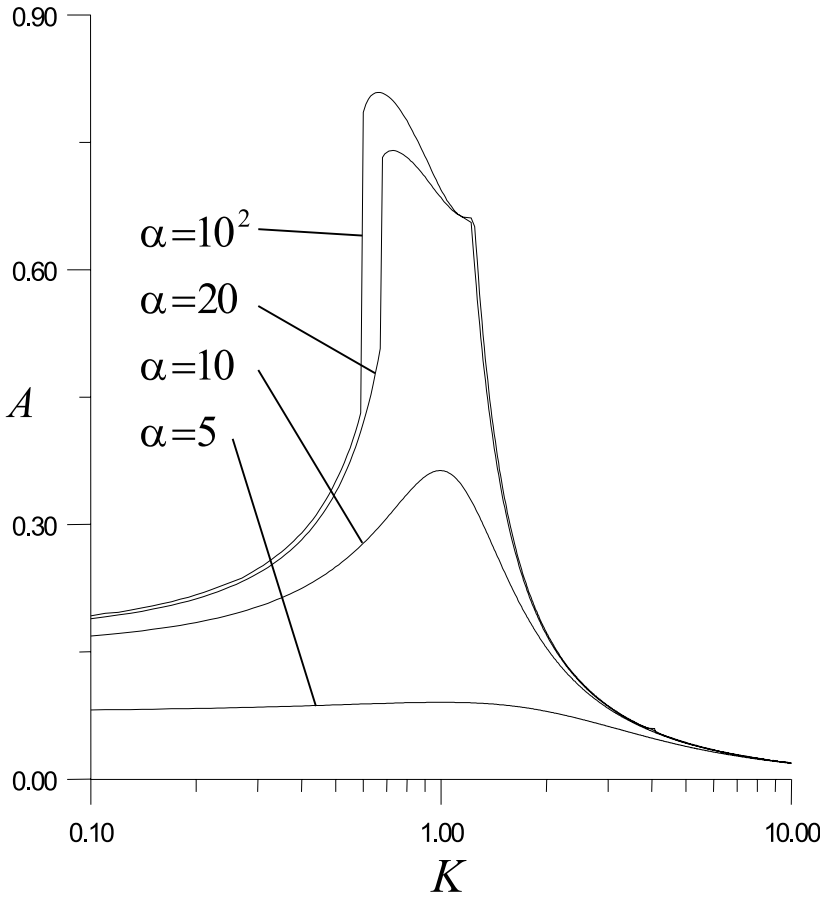

Figure 8

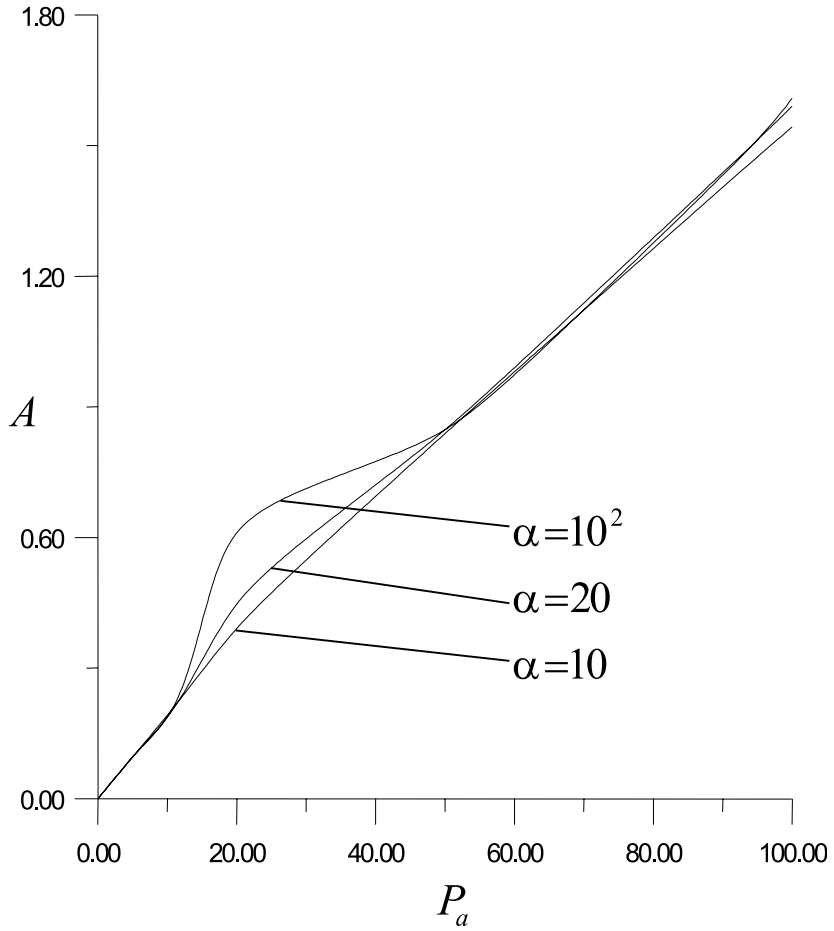
1.80
1.20
0.60
0.00
A
0.00
20.00
40.00
60.00
80.00
100.00
P_a
$\alpha=10^2$
$\alpha=20$
$\alpha=10$

Figure 9

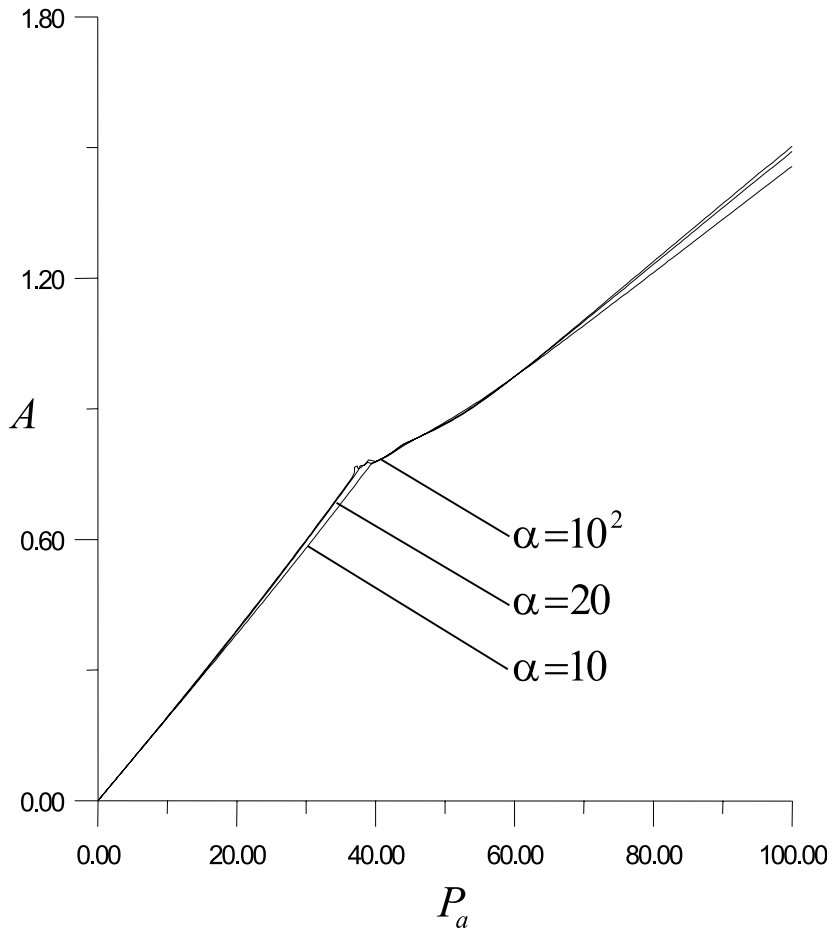
1.80
1.20
0.60
0.00
A
0.00
20.00
40.00
60.00
80.00
100.00
P_a
$\alpha=10^2$
$\alpha=20$
$\alpha=10$